

Equation of state and electrical transport properties of mixture
of $\text{Li}_{1.2}\text{Mn}_{0.54}\text{Co}_{0.13}\text{Ni}_{0.13}\text{O}_2$ and $\text{LiNi}_{0.87}\text{Co}_{0.09}\text{Mn}_{0.03}\text{Al}_{0.01}\text{O}_2$
at high pressure

HPSTAR
1331-2021

Lun Xiong*,[¶] Pu Tu*, Yongqing Hu*, Xiang Hou*, Shiyun Wu*,
Xingquan Liu[†], Hongliang Dong^{‡,§} and Ziyou Zhang[‡]

**School of Intelligent Manufacturing,
Sichuan University of Arts and Science,
Dazhou 635000, P. R. China*

*†School of Materials and Energy,
University of Electronic Science and Technology,
Chengdu 610054, P. R. China*

*‡Center for High Pressure Science and Technology Advanced Research,
Pudong, Shanghai 201203, P. R. China*

*§State Key Laboratory of High Performance Ceramics and
Superfine Microstructure,
Shanghai Institute of Ceramics, Chinese Academy of Sciences,
Shanghai 201899, P. R. China*

¶1094129778@qq.com

Received 20 April 2021
Revised 8 June 2021
Accepted 2 July 2021
Published 5 August 2021

The equation of state (EOS) of mixture of $\text{Li}_{1.2}\text{Mn}_{0.54}\text{Co}_{0.13}\text{Ni}_{0.13}\text{O}_2$ and $\text{LiNi}_{0.87}\text{Co}_{0.09}\text{Mn}_{0.03}\text{Al}_{0.01}\text{O}_2$ was studied by synchrotron radiation X-ray diffraction (XRD) at room-temperature in a diamond anvil cell (DAC). The results showed that the hexagonal structure is maintained to the highest pressure of 23.1 GPa. The bulk modulus and its first derivative obtained from XRD data are $K_0 = 147.4(3.1)$ GPa and $K'_0 = 2.21(0.33)$, respectively. In addition, we have investigated the high-pressure electrical conductivity of the mixture of $\text{Li}_{1.2}\text{Mn}_{0.54}\text{Co}_{0.13}\text{Ni}_{0.13}\text{O}_2$ and $\text{LiNi}_{0.87}\text{Co}_{0.09}\text{Mn}_{0.03}\text{Al}_{0.01}\text{O}_2$ to 22.9 GPa in a DAC. It is found that the resistance decreases with the increase of pressure and changes exponentially.

Keywords: $\text{Li}_{1.2}\text{Mn}_{0.54}\text{Co}_{0.13}\text{Ni}_{0.13}\text{O}_2$; $\text{LiNi}_{0.87}\text{Co}_{0.09}\text{Mn}_{0.03}\text{Al}_{0.01}\text{O}_2$; equation of state; electrical transport properties; high pressure.

PACS numbers: 07.35.+k, 61.05.cp, 64.30.Jk, 72.80.-r

[¶]Corresponding author.

1. Introduction

Lithium-ion battery is widely used in new energy electric vehicles and small electronic products due to its advantages of high capacity, long life and environmental friendliness. Looking for a new cathode material with low price, safety and environmental protection and high discharge capacity has become a research hotspot of lithium-ion battery. In recent years, with the requirements of miniaturization of digital products and high driving range of new energy vehicles, the energy density of lithium-ion batteries is required to be higher and higher. The common cathode materials for lithium-ion batteries are LiMO_2 ($M=\text{Co}, \text{Ni}$, etc.),¹⁻⁴ LiMn_2O_4 ,⁵⁻¹⁰ LiFePO_4 ,¹¹⁻¹³ $\text{Li}(\text{NiMn})\text{O}_2$,^{14,15} $\text{LiNi}_{1-x-y}\text{Co}_x\text{Mn}_y\text{O}_2$ ^{16,17} and $x\text{Li}_2\text{MnO}_3 \cdot (1-x)\text{LiMO}_2$ ($M=\text{Ni}, \text{Co}, \text{Mn}$, etc.).¹⁸⁻²⁵ In recent years, the lithium rich manganese based cathode material $x\text{Li}_2\text{MnO}_3 \cdot (1-x)\text{LiMO}_2$ ($M=\text{Ni}, \text{Co}, \text{Mn}$, etc.) combines the advantages of several materials, such as high specific capacity, high voltage and high-energy density, and becomes the key research object of high-energy density materials. The specific capacity of lithium rich manganese based cathode materials is as high as 250 mAh/g, which is close to twice that of traditional cathode materials. In addition, the cost of lithium-ion battery can be greatly reduced and the environmental pollution can be reduced by using lithium rich manganese based cathode materials instead of expensive lithium cobalt oxide and lithium nickel oxide. Lithium rich manganese based materials also have the advantages of high safety and simple production process. Therefore, lithium rich manganese based cathode material is a promising cathode material. It can be predicted that lithium-ion batteries with lithium rich manganese based cathode materials will be widely used in a series of fields in the future. Lithium rich manganese based cathode materials are good substitutes for LiCoO_2 and LiFePO_4 , which are the main commercial cathode products at present.

The excellent electrochemical performance of lithium rich manganese based cathode materials depends on their unique crystal structure and charge discharge mechanism. $x\text{Li}_2\text{MnO}_3 \cdot (1-x)\text{LiMO}_2$ ($M=\text{Ni}, \text{Co}, \text{Mn}$, etc.) can be regarded as a solid solution composed of Li_2MnO_3 and LiMO_2 . Li_2MnO_3 is a rock salt structure (monoclinic) with a space group $C2/m$, LiMO_2 is a hexagonal crystal system with space group $R-3m$, and has the same structure as the crystal $\alpha\text{-NaFeO}_2$. $\text{Li}_{1.2}\text{Mn}_{0.54}\text{Co}_{0.13}\text{Ni}_{0.13}\text{O}_2$ is composed of Li_2MnO_3 and LiMO_2 ($M=\text{Ni}, \text{Co}, \text{Mn}$, etc.) with the same proportion, and has a layered structure compared with $\alpha\text{-NaFeO}_2$. It has excellent electrochemical properties such as high capacity, good cycle stability and market advantages (such as low cost, safety and environmental protection). It is a very promising commercial cathode material at present.

As a basic parameter of thermodynamics, pressure plays an important role in the study of condensed matter. It can change the distance between atoms in matter, make atoms pile up in a more compact way, and then change its structure and physical, chemical and other related properties, such as high-pressure structural phase transition, high-pressure strength and high-pressure texture.²⁶ High pressure

science is an interdisciplinary science. With the development of high pressure technology, it has been integrated with physics, materials science, chemistry, geosciences and other disciplines, which has greatly promoted the application and development of itself and its related fields. It is an important field of basic research and applied science research. Pressure can also increase or decrease the overlap of electron wavefunctions, which will eventually lead to structural phase transition, electronic structural phase transition and new band structure. It is difficult to observe these phenomena at the micro level, but they can be reflected in the detected electrical properties, mainly in the changes of physical parameters such as resistivity, carrier behavior, Hall coefficient and so on. Using high-pressure *in situ* electrical measurement experiment, can help us to, effectively and comprehensively, understand the change of material properties under pressure and master its law. At present, there are some researches on the experimental research and theoretical calculation of cathode materials for lithium-ion batteries under high pressure. For example, Arroyo-deDompablo *et al.*²⁷ studied the electrical properties of LiFePO_4 treated by high pressure and high-temperature through experiments and theoretical calculation. The results show that the samples treated by high-temperature and high pressure have better electronic conductivity, but the lithium-ion conductivity is poor. Fell *et al.*²⁸ studied the electrochemical properties of $\text{LiNi}_x\text{Co}_y\text{Mn}_z\text{O}_2$ treated by high pressure and high-temperature. It was found that the structure of the cathode material changed after high pressure treatment, and the electrochemical properties of the cathode material after high pressure treatment were different from those before high pressure treatment. These studies have important guiding significance for the research, improvement and application of the electrochemical performance of cathode materials for lithium-ion batteries.

Despite of many reports about lithium rich manganese based cathode materials,^{18–25} the high-pressure structure and electrical transport properties have not been reported. In this paper, the equation of state (EOS) and structural phase transition of the mixture of $\text{Li}_{1.2}\text{Mn}_{0.54}\text{Co}_{0.13}\text{Ni}_{0.13}\text{O}_2$ and $\text{LiNi}_{0.87}\text{Co}_{0.09}\text{Mn}_{0.03}\text{Al}_{0.01}\text{O}_2$ to 23.1 GPa were studied by synchrotron radiation X-ray diffraction (XRD), and the high-pressure resistance of the mixture of $\text{Li}_{1.2}\text{Mn}_{0.54}\text{Co}_{0.13}\text{Ni}_{0.13}\text{O}_2$ and $\text{LiNi}_{0.87}\text{Co}_{0.09}\text{Mn}_{0.03}\text{Al}_{0.01}\text{O}_2$ to 22.9 GPa was studied in a diamond anvil cell (DAC) by AC impedance method.

2. Experimental Details

The crystal structures of $\text{Li}_{1.2}\text{Mn}_{0.54}\text{Co}_{0.13}\text{Ni}_{0.13}\text{O}_2$ and $\text{LiNi}_{0.87}\text{Co}_{0.09}\text{Mn}_{0.03}\text{Al}_{0.01}\text{O}_2$ are hexagonal at ambient conditions. The space group is R-3m (shown in Fig. 1). We can determine the proportion of each element by inductively coupled plasma (ICP) method. In addition, $\text{Li}_{1.2}\text{Mn}_{0.54}\text{Co}_{0.13}\text{Ni}_{0.13}\text{O}_2$ and $\text{LiNi}_{0.87}\text{Co}_{0.09}\text{Mn}_{0.03}\text{Al}_{0.01}\text{O}_2$ were mixed by mechanical ball milling at a mass ratio of 1:1. Scanning electron microscope (SEM) test was completed in the analysis and testing center of Sichuan University. The SEM instrument model is

L. Xiong et al.

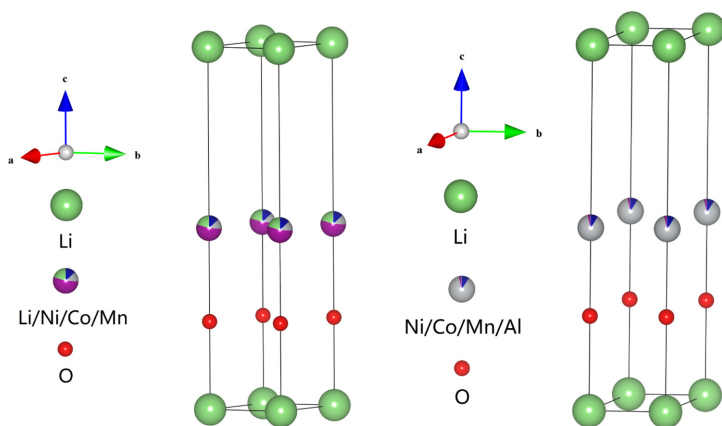


Fig. 1. (Color online) The crystal structures of $\text{Li}_{1.2}\text{Mn}_{0.54}\text{Co}_{0.13}\text{Ni}_{0.13}\text{O}_2$ and $\text{LiNi}_{0.87}\text{Co}_{0.09}\text{Mn}_{0.03}\text{Al}_{0.01}\text{O}_2$ studied at ambient pressure, respectively.

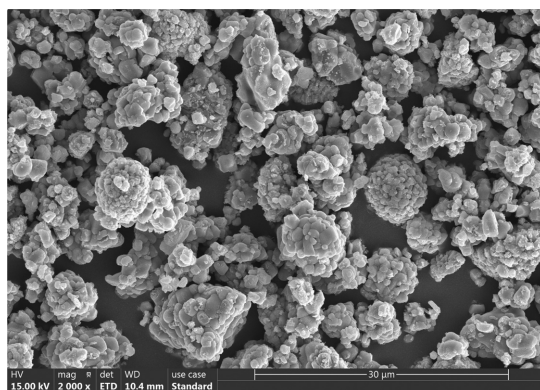


Fig. 2. SEM image of mixture of $\text{Li}_{1.2}\text{Mn}_{0.54}\text{Co}_{0.13}\text{Ni}_{0.13}\text{O}_2$ and $\text{LiNi}_{0.87}\text{Co}_{0.09}\text{Mn}_{0.03}\text{Al}_{0.01}\text{O}_2$ sample at ambient pressure.

JSM-7500F, resolution is 1.0 nm (15 kV), magnification is 25–800,000. It can be seen that the average cluster size of the original $\text{Li}_{1.2}\text{Mn}_{0.54}\text{Co}_{0.13}\text{Ni}_{0.13}\text{O}_2$ and $\text{LiNi}_{0.87}\text{Co}_{0.09}\text{Mn}_{0.03}\text{Al}_{0.01}\text{O}_2$ mixture is 10 μm (see Fig. 2). XRD experiment of copper target was also completed in the analysis and testing center of Sichuan University. The model of X-ray diffractometer is EMPYREAN, the minimum controllable step is 0.0001° , the resolution is $\text{FWHM} = 0.028^\circ$. The wavelength of XRD of copper target is 1.5406 \AA , and the diffraction spectrum of mixture of $\text{Li}_{1.2}\text{Mn}_{0.54}\text{Co}_{0.13}\text{Ni}_{0.13}\text{O}_2$ and $\text{LiNi}_{0.87}\text{Co}_{0.09}\text{Mn}_{0.03}\text{Al}_{0.01}\text{O}_2$ obtained at room-temperature and room pressure is shown in Fig. 3. It can be seen that the diffraction peaks of mixture of $\text{Li}_{1.2}\text{Mn}_{0.54}\text{Co}_{0.13}\text{Ni}_{0.13}\text{O}_2$ and $\text{LiNi}_{0.87}\text{Co}_{0.09}\text{Mn}_{0.03}\text{Al}_{0.01}\text{O}_2$ almost coincide, indicating that they have the same crystal structure and very close cell parameters. The derived lattice

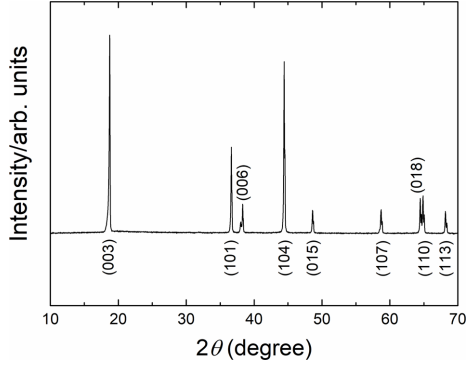


Fig. 3. The representative powder XRD of mixture of $\text{Li}_{1.2}\text{Mn}_{0.54}\text{Co}_{0.13}\text{Ni}_{0.13}\text{O}_2$ and $\text{LiNi}_{0.87}\text{Co}_{0.09}\text{Mn}_{0.03}\text{Al}_{0.01}\text{O}_2$ at ambient conditions. The corresponding Miller indices are noted for each peak.

parameters of $\text{Li}_{1.2}\text{Mn}_{0.54}\text{Co}_{0.13}\text{Ni}_{0.13}\text{O}_2$ and $\text{LiNi}_{0.87}\text{Co}_{0.09}\text{Mn}_{0.03}\text{Al}_{0.01}\text{O}_2$ are $a = 2.87268(0.00033)$ Å and $c = 14.19418(0.00275)$ Å, and $a = 2.86494(0.00033)$ Å and $c = 14.17511(0.00275)$ Å, respectively. High-pressure XRD experiments were carried out in a modified Mao Bell DAC with a diameter of 300 μm . A T301 gasket was pre-pressed to a thickness of about 35 μm , and then a sample hole with a diameter of 120 μm was drilled in the middle of the indentation. The pressure transition medium of this experiment is silicone oil. We use a ruby chip with a diameter of ~ 10 μm as a pressure sensor.²⁹

In situ high-pressure XRD experiments were conducted at BL15U1 beam line of Shanghai Synchrotron Radiation Facility (SSRF). The wavelength of the beam line is 0.6199 Å. The diffraction spectrum is received by a MarCCD detector, and the distance from the detector to the sample and the deflection angle of the detector are calibrated by CeO_2 . The exposure time of each XRD spectrum is 1–3 min. Then, we use fit2d software³⁰ for processing and analysis.

In situ high-pressure transport measurements of mixture of $\text{Li}_{1.2}\text{Mn}_{0.54}\text{Co}_{0.13}\text{Ni}_{0.13}\text{O}_2$ and $\text{LiNi}_{0.87}\text{Co}_{0.09}\text{Mn}_{0.03}\text{Al}_{0.01}\text{O}_2$ were carried out in a DAC, and the sample was compressed in the DAC. In order to load the sample into the DAC, we pre-pressed the T301 gasket to a thickness of 30 μm . Then we drilled a sample hole with a diameter of 250 μm in the middle of the indentation of the gasket. A thin layer of cubic boron nitride (cBN) is pressed onto the gasket to insulate the electrode from the gasket. Then we drilled a 130 μm diameter hole in the middle of the cBN to load the powder sample into the DAC. In order to ensure the good conductivity between the electrode and the sample and prevent the introduction of possible impurities and electrode short circuit, no pressure medium was added in the experiment. AC impedance is used to measure electrical transmission.³¹ The method is to connect two electrodes to the sample and measure the AC impedance pattern in the DAC. The AC impedance spectra was measured using the CS353 impedance analyzer (Wuhan Keruite Instrument Co., Ltd.) in the frequency range

of 0.01 Hz to 10 MHz. After the data modeling, the resistance of the sample is measured in Ohms.

3. Results and Discussion

We use fit2d software³⁰ to process and analyze the diffraction spectrum of mixture of $\text{Li}_{1.2}\text{Mn}_{0.54}\text{Co}_{0.13}\text{Ni}_{0.13}\text{O}_2$ and $\text{LiNi}_{0.87}\text{Co}_{0.09}\text{Mn}_{0.03}\text{Al}_{0.01}\text{O}_2$. The maximum pressure of high-pressure XRD experiment is 23.1 GPa, and the pressure is obtained by ruby pressure standard.²⁹ Figure 4 shows the diffraction patterns of mixture of $\text{Li}_{1.2}\text{Mn}_{0.54}\text{Co}_{0.13}\text{Ni}_{0.13}\text{O}_2$ and $\text{LiNi}_{0.87}\text{Co}_{0.09}\text{Mn}_{0.03}\text{Al}_{0.01}\text{O}_2$ mixture at different pressures. It can be seen that (003), (101), (006), (104) and (015) diffraction peaks can be observed in the whole pressure range. It can also be seen that the diffraction peaks of mixture of $\text{Li}_{1.2}\text{Mn}_{0.54}\text{Co}_{0.13}\text{Ni}_{0.13}\text{O}_2$ and $\text{LiNi}_{0.87}\text{Co}_{0.09}\text{Mn}_{0.03}\text{Al}_{0.01}\text{O}_2$ coincide. Thus, we can obtain the unique cell parameters for both of $\text{Li}_{1.2}\text{Mn}_{0.54}\text{Co}_{0.13}\text{Ni}_{0.13}\text{O}_2$ and $\text{LiNi}_{0.87}\text{Co}_{0.09}\text{Mn}_{0.03}\text{Al}_{0.01}\text{O}_2$.

The lattice parameters and volumes of $\text{Li}_{1.2}\text{Mn}_{0.54}\text{Co}_{0.13}\text{Ni}_{0.13}\text{O}_2$ and $\text{LiNi}_{0.87}\text{Co}_{0.09}\text{Mn}_{0.03}\text{Al}_{0.01}\text{O}_2$ mixture under different pressures were fitted by the d -spacings of $d(003)$, $d(101)$, $d(006)$, $d(104)$ and $d(015)$. The a -axis, c -axis and c/a compressibility of mixture of $\text{Li}_{1.2}\text{Mn}_{0.54}\text{Co}_{0.13}\text{Ni}_{0.13}\text{O}_2$ and $\text{LiNi}_{0.87}\text{Co}_{0.09}\text{Mn}_{0.03}\text{Al}_{0.01}\text{O}_2$ are shown in Fig. 5. The results show that the a and c parameters of hexagonal phase decrease with the increase of pressure. The results show that the unit cell parameters of $\text{Li}_{1.2}\text{Mn}_{0.54}\text{Co}_{0.13}\text{Ni}_{0.13}\text{O}_2$ and $\text{LiNi}_{0.87}\text{Co}_{0.09}\text{Mn}_{0.03}\text{Al}_{0.01}\text{O}_2$ mixture change continuously in the whole pressure range. However, c/a is discontinuous in the whole pressure range of the experimental results. The binomial function of the whole pressure range is given

$$a = 2.87736 - 0.00613P + 0.0000100341P^2 \quad (1)$$

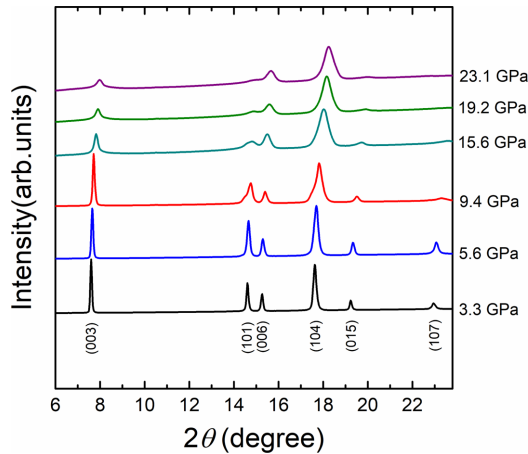


Fig. 4. (Color online) Normalized XRD patterns of mixture of $\text{Li}_{1.2}\text{Mn}_{0.54}\text{Co}_{0.13}\text{Ni}_{0.13}\text{O}_2$ and $\text{LiNi}_{0.87}\text{Co}_{0.09}\text{Mn}_{0.03}\text{Al}_{0.01}\text{O}_2$ under different pressures.

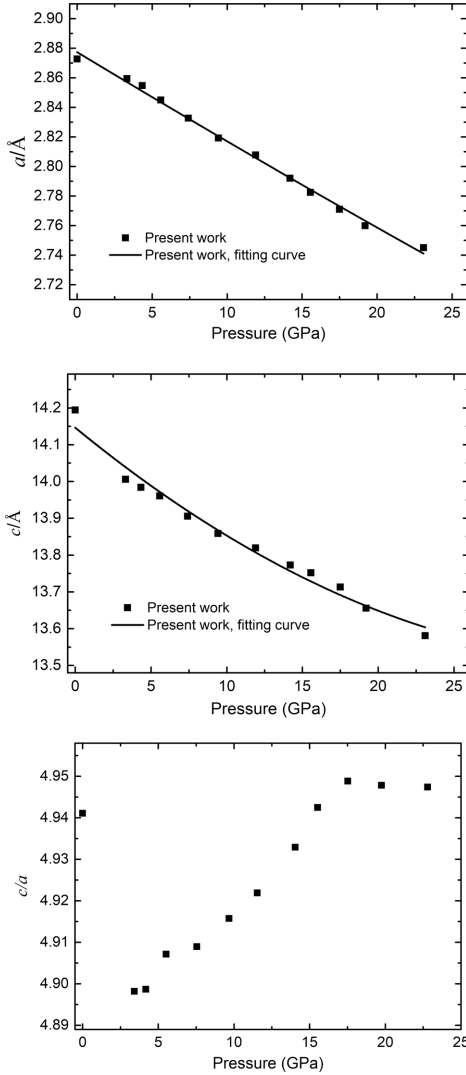


Fig. 5. Lattice parameters and c/a of mixture of $\text{Li}_{1.2}\text{Mn}_{0.54}\text{Co}_{0.13}\text{Ni}_{0.13}\text{O}_2$ and $\text{LiNi}_{0.87}\text{Co}_{0.09}\text{Mn}_{0.03}\text{Al}_{0.01}\text{O}_2$ at high pressure.

and

$$c = 14.1465 - 0.03381P + 0.000446587P^2. \quad (2)$$

The compression curve of high-pressure XRD experiment is shown in Fig. 6. The results show that the hexagonal structure of mixture of $\text{Li}_{1.2}\text{Mn}_{0.54}\text{Co}_{0.13}\text{Ni}_{0.13}\text{O}_2$ and $\text{LiNi}_{0.87}\text{Co}_{0.09}\text{Mn}_{0.03}\text{Al}_{0.01}\text{O}_2$ is maintained to the highest pressure of 23.1 GPa.

We use the third-order Birch–Murnaghan equation to fit the volume change data under high pressure. From this, we can get the bulk modulus of K_0 and its first

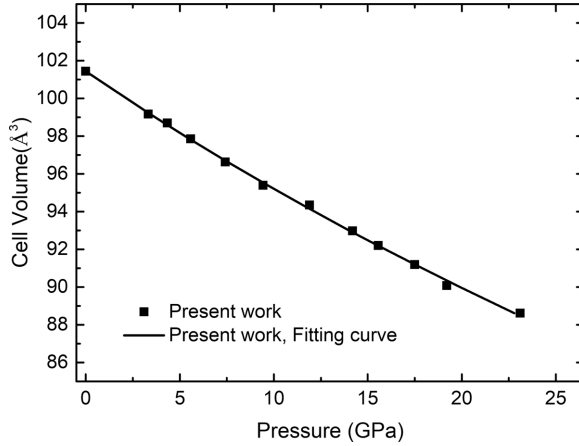


Fig. 6. Compression curves of mixture of $\text{Li}_{1.2}\text{Mn}_{0.54}\text{Co}_{0.13}\text{Ni}_{0.13}\text{O}_2$ and $\text{LiNi}_{0.87}\text{Co}_{0.09}\text{Mn}_{0.03}\text{Al}_{0.01}\text{O}_2$ under high pressure. The lines are Birch–Murnaghan fitting based on the experimental data.

derivative of K'_0 . The third-order Birch–Murnaghan equation can be expressed as³²

$$P = 1.5K_0 \left[\left(\frac{V_0}{V} \right)^{\frac{7}{3}} - \left(\frac{V_0}{V} \right)^{\frac{5}{3}} \right] \left\{ 1 + \frac{3}{4}(K'_0 - 4) \left[\left(\frac{V_0}{V} \right)^{\frac{2}{3}} - 1 \right] \right\}, \quad (3)$$

where K_0 , K'_0 and V_0 are the bulk modulus, the pressure derivate of bulk modulus and the volume at ambient conditions, respectively.

The bulk modulus of mixture of $\text{Li}_{1.2}\text{Mn}_{0.54}\text{Co}_{0.13}\text{Ni}_{0.13}\text{O}_2$ and $\text{LiNi}_{0.87}\text{Co}_{0.09}\text{Mn}_{0.03}\text{Al}_{0.01}\text{O}_2$ obtained from XRD data is $K_0 = 147.4(3.1)$ GPa with $K'_0 = 2.21(0.33)$. The comparison between the present results and the previously reported bulk modulus and pressure derivative of hexagonal structure cathode materials for lithium-ion batteries is shown in Table 1. It can be seen that the zero pressure bulk modulus of the mixture of $\text{Li}_{1.2}\text{Mn}_{0.54}\text{Co}_{0.13}\text{Ni}_{0.13}\text{O}_2$ and $\text{LiNi}_{0.87}\text{Co}_{0.09}\text{Mn}_{0.03}$

Table 1. Summary of the bulk modulus (K_0) and its pressure derivative (K'_0) of hexagonal structure of cathode materials for lithium-ion batteries (mixture of $\text{Li}_{1.2}\text{Mn}_{0.54}\text{Co}_{0.13}\text{Ni}_{0.13}\text{O}_2$ and $\text{LiNi}_{0.87}\text{Co}_{0.09}\text{Mn}_{0.03}\text{Al}_{0.01}\text{O}_2$, $\text{LiNi}_{0.8}\text{Co}_{0.1}\text{Mn}_{0.1}\text{O}_2$ and LiCoO_2) derived from various methods.

Sample	K_0 (GPa)	K'_0	Method	PTM	Ref.
Mixture	147.4(3.1)	2.21(0.33)	XRD	Si oil	Present work
$\text{LiNi}_{0.8}\text{Co}_{0.1}\text{Mn}_{0.1}\text{O}_2$	126.2(4.2)	8.58(0.84)	XRD	Si oil	Xiong <i>et al.</i> ³³
LiCoO_2	159.5(2.2)	3.92(0.23)	XRD	So oil	Hu <i>et al.</i> ³⁴
	118.5	4(fixed)	XRD	So oil	Xu <i>et al.</i> ³
	149(2)	4.1(0.3)	XRD	Nitrogen	Wang <i>et al.</i> ³⁵
	166.74	—	GGA	—	Wu <i>et al.</i> ³⁶

Note: Mixture refers to mixture of $\text{Li}_{1.2}\text{Mn}_{0.54}\text{Co}_{0.13}\text{Ni}_{0.13}\text{O}_2$ and $\text{LiNi}_{0.87}\text{Co}_{0.09}\text{Mn}_{0.03}\text{Al}_{0.01}\text{O}_2$; PTM refers to pressure transition medium; Si oil refers to silicone oil; GGA refers to the generalized gradient approximation.

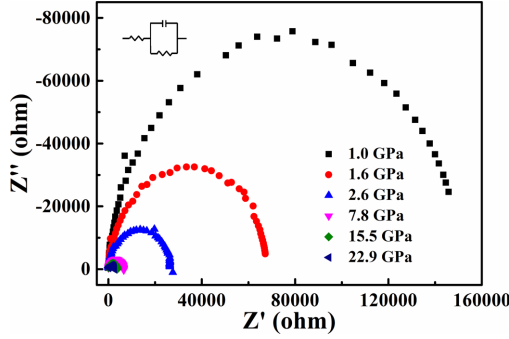


Fig. 7. (Color online) Selected Nyquist plots of AC impedance spectroscopy of mixture of $\text{Li}_{1.2}\text{Mn}_{0.54}\text{Co}_{0.13}\text{Ni}_{0.13}\text{O}_2$ and $\text{LiNi}_{0.87}\text{Co}_{0.09}\text{Mn}_{0.03}\text{Al}_{0.01}\text{O}_2$ upto 22.9 GPa.

$\text{Al}_{0.01}\text{O}_2$ in this work is close to that of LiCoO_2 , but slightly larger than that of $\text{LiNi}_{0.8}\text{Co}_{0.1}\text{Mn}_{0.1}\text{O}_2$.

In this study, AC impedance spectroscopy was combined with DAC technology to measure the *in situ* resistance of mixture of $\text{Li}_{1.2}\text{Mn}_{0.54}\text{Co}_{0.13}\text{Ni}_{0.13}\text{O}_2$ and $\text{LiNi}_{0.87}\text{Co}_{0.09}\text{Mn}_{0.03}\text{Al}_{0.01}\text{O}_2$ at high pressure. The experimental results of Nyquist plots are shown in Fig. 7. It can be seen that the radius of impedance spectrum decreases with the increase of pressure, which indicates that the grain resistance of $\text{Li}_{1.2}\text{Mn}_{0.54}\text{Co}_{0.13}\text{Ni}_{0.13}\text{O}_2$ and $\text{LiNi}_{0.87}\text{Co}_{0.09}\text{Mn}_{0.03}\text{Al}_{0.01}\text{O}_2$ mixture decreases.

The equivalent electrical circuit is used to simulate the AC impedance spectroscopy to describe the relaxation process in the grain boundary. By fitting the AC impedance spectrum to the circuit model (using ZView software), the circuit parameters were obtained. The exponential function fitting results in Fig. 8 show that, below ~ 2.6 GPa, the grain (bulk) resistance of the sample decreases significantly and presents a continuous change with the increase of pressure. The fitting result of the whole compression pressure range is as follows

$$y = 152798.8P^{-1.70787}. \quad (4)$$

As a comparison, exponential function is used to fit the whole decompression pressure range, and the result is obtained as

$$y = 37464P^{-0.83114}. \quad (5)$$

It can be seen that the resistance changes greatly during compression, similar to that from semiconductor to conductor. Pressure will modulate the crystal structure and electronic structure, resulting in changes in resistance.^{37,38} According to the synchrotron radiation XRD experiments, we found no crystal structure change until the maximum pressure of 23.1 GPa. The rapid change of resistance can be attributed to the broadening of valence band and conduction band, which is caused by the shortening and bending of bonds.^{39–41} Over 2.6 GPa, the slow change of resistance is attributed to the change of electronic structure, which can be found in semiconductors without structural phase transition at high pressure.^{42,43}

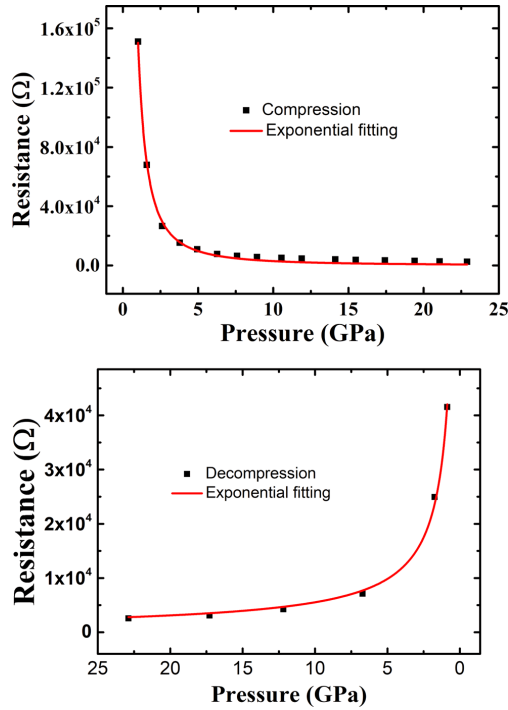


Fig. 8. (Color online) Pressure dependence of the grain resistance of mixture of $\text{Li}_{1.2}\text{Mn}_{0.54}\text{Co}_{0.13}\text{Ni}_{0.13}\text{O}_2$ and $\text{LiNi}_{0.87}\text{Co}_{0.09}\text{Mn}_{0.03}\text{Al}_{0.01}\text{O}_2$ measured from AC impedance spectroscopy during (a) compression process and (b) decompression process.

4. Conclusion

In conclusion, we have studied the EOS and structural phase transition of $\text{Li}_{1.2}\text{Mn}_{0.54}\text{Co}_{0.13}\text{Ni}_{0.13}\text{O}_2$ and $\text{LiNi}_{0.87}\text{Co}_{0.09}\text{Mn}_{0.03}\text{Al}_{0.01}\text{O}_2$ mixture to 23.1 GPa in the quasi-hydrostatic environment in a DAC. It is found that the hexagonal structure of the mixture of $\text{Li}_{1.2}\text{Mn}_{0.54}\text{Co}_{0.13}\text{Ni}_{0.13}\text{O}_2$ and $\text{LiNi}_{0.87}\text{Co}_{0.09}\text{Mn}_{0.03}\text{Al}_{0.01}\text{O}_2$ is maintained upto the maximum pressure of 23.1 GPa without phase transition. The bulk modulus of material obtained from XRD data is 147.4(3.1) GPa, and the first derivative of bulk modulus is 2.21(0.33). In addition, we have also studied the high-pressure resistance of the mixture of $\text{Li}_{1.2}\text{Mn}_{0.54}\text{Co}_{0.13}\text{Ni}_{0.13}\text{O}_2$ and $\text{LiNi}_{0.87}\text{Co}_{0.09}\text{Mn}_{0.03}\text{Al}_{0.01}\text{O}_2$ to 22.9 GPa in DAC using AC impedance method. The results show that the resistance is exponentially continuous with the change of pressure.

Acknowledgments

This work was supported by the Project of Ph.D special research of Sichuan University of Arts and Science, China (No. 2019BS006Z) and the Open fund project of

Industrial Technology Institute of School of Intelligent Manufacturing of Sichuan University of Arts and Science, China (No. ZNZZ2101). The synchrotron radiation XRD experiment in this work was performed at BL15U1 beamline of Shanghai Synchrotron Radiation Facility (SSRF).

References

1. J. N. Reimers and J. R. Dahn, *J. Electrochem. Soc.* **139**, 2091 (1992).
2. B. Huang *et al.*, *J. Appl. Electrochem.* **28**, 1365 (1998).
3. C. Xu, F. Sun and W. G. Yang, *Chin. J. High Press. Phys.* **31**, 529 (2017).
4. C. Wolverton and A. Zunger, *J. Electrochem. Soc.* **145**, 2424 (1998).
5. A. Paolone *et al.*, *Solid State Ionics* **176**, 635 (2005).
6. K. Yamaura *et al.*, *J. Am. Chem. Soc.* **128**, 9448 (2006).
7. P. Piszora, *Z. Kristallogr.* **26**, 387 (2007).
8. P. Piszora, *Solid State Phenom.* **130**, 69 (2007).
9. P. Piszora *et al.*, *Radiat. Phys. Chem.* **78**, S89 (2009).
10. J. Daru *et al.*, *Radiat. Phys. Chem.* **80**, 1014 (2011).
11. O. Garciamoreno *et al.*, *Chem. Mater.* **13**, 1570 (2001).
12. L. He and Z. Zeng, *IEEE Trans. Magn.* **47**, 3817 (2011).
13. H. N. Dong *et al.*, *Solid State Ionics* **301**, 133 (2017).
14. J. Xiao *et al.*, *Adv. Mater.* **24**, 2109 (2012).
15. L. P. Wang *et al.*, *Solid State Ionics* **193**, 32 (2011).
16. C. R. Fell *et al.*, *Energy Environ. Sci.* **5**, 6214 (2012).
17. L. Z. Liu, A. Yu and Y. L. Jim, *J. Power Sources* **81**, 416 (1999).
18. Z. H. Lu and J. R. Dahn, Cathode compositions for lithium-ion batteries, US Patent No. 6964828 (2005).
19. M. M. Thackeray, C. S. Johnson and K. Amine Lithium metal oxide electrodes for lithium cells and batteries, US Patent No. 6677082 (2002).
20. C. S. Johnson *et al.*, *Electrochem. Commun.* **6**, 2313 (2004).
21. S. H. Park *et al.*, *Mater. Chem. Phys.* **102**, 225 (2007).
22. C. Yu *et al.*, *Phys. Chem. Chem. Phys.* **14**, 12368 (2012).
23. R. Wang *et al.*, *Adv. Energy Mater.* **3**, 1358 (2013).
24. Y. C. Kan *et al.*, *J. Power Sources* **266**, 341 (2014).
25. L. G. Wang *et al.*, *J. Am. Chem. Soc.* **142**, 14966 (2020).
26. L. Xiong *et al.*, *Int. J. Mod. Phys. B* **32**, 1850177 (2018).
27. M. E. Arroyo-de Dompablo, J. M. Gallardo-Amores and U. Amador, *Electrochem. Solid-State Lett.* **8**, A564 (2005).
28. C. R. Fell *et al.*, *Energ. Environ. Sci.* **5**, 6214 (2012).
29. H. K. Mao, J. Xu and P. M. Bell, *J. Geophys. Res.* **91**, 4673 (1986).
30. A. P. Hammersley *et al.*, *High Press. Res.* **14**, 235 (1996).
31. J. X. Liu *et al.*, *J. Phys. Chem. C* **123**, 4094 (2019).
32. F. Birch, *J. Geophys. Res.* **83**, 1257 (1978).
33. L. Xiong *et al.*, *Solid State Commun.* **299**, 113656 (2019).
34. Y. Q. Hu *et al.*, *Chin. Phys. B* **28**, 016402 (2019).
35. X. Wang *et al.*, *Phys. Rev. B* **72**, 224102 (2005).
36. L. M. Wu and J. Zhang, *J. Appl. Phys.* **118**, 225101 (2015).
37. Y. Wang *et al.*, *J. Am. Chem. Soc.* **137**, 11144 (2015).
38. G. Zhang *et al.*, *Adv. Electron. Mater.* **3**, 1600498 (2017).

L. Xiong et al.

39. Y. Ma *et al.*, *Nature* **458**, 182 (2009).
40. K. Arai *et al.*, *J. Non-Cryst. Solids* **13**, 131 (1973).
41. G. H. Zhang *et al.*, *J. Mater. Chem. A* **7**, 4019 (2019).
42. Z. Zhao *et al.*, *Nat. Commun.* **6**, 7312 (2015).
43. Y. Wang *et al.*, *J. Am. Chem. Soc.* **138**, 15751 (2016).